Lawrence Berkeley National Laboratory
LBL Publications

Title
Time-Dependent Density-Matrix Theory II. Mass Dispersion in Damped Nuclear Reactions

Permalink
https://escholarship.org/uc/item/3gf164p8

Authors
Gong, M.
Tohyama, M.
Randrup, Jorgen

Publication Date
1989-10-01

eScholarship.org Powered by the California Digital Library
University of California

LBL-27820
Preprint

Lawrence Berkeley Laboratory
UNIVERSITY OF CALIFORNIA

Submitted to Zeitschrift für Physik

Time-Dependent Density-Matrix Theory

II. Mass Dispersion in Damped Nuclear Reactions

M. Gong, M. Tohyama, and J. Randrup

October 1989

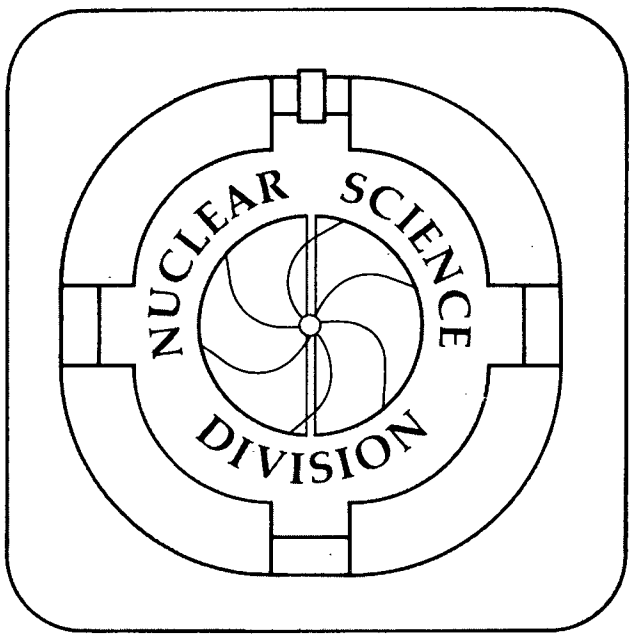

Prepared for the U.S. Department of Energy under Contract Number DE-AC03-76SF00098.

LOAN COPY
Circulates
for 2 weeks
Bldg. 50 Library.
Copy 2
LBL-27820

DISCLAIMER

This document was prepared as an account of work sponsored by the United States Government. While this document is believed to contain correct information, neither the United States Government nor any agency thereof, nor the Regents of the University of California, nor any of their employees, makes any warranty, express or implied, or assumes any legal responsibility for the accuracy, completeness, or usefulness of any information, apparatus, product, or process disclosed, or represents that its use would not infringe privately owned rights. Reference herein to any specific commercial product, process, or service by its trade name, trademark, manufacturer, or otherwise, does not necessarily constitute or imply its endorsement, recommendation, or favoring by the United States Government or any agency thereof, or the Regents of the University of California. The views and opinions of authors expressed herein do not necessarily state or reflect those of the United States Government or any agency thereof or the Regents of the University of California.

LBL-27820

Time-Dependent Density-Matrix Theory

II. Mass Dispersion in Damped Nuclear Reactions*

M. Gong and *M. Tohyama*
NSCL and Physics Department, Michigan State University
East Lansing, Michigan 48824-1321

and

J. Randrup
Nuclear Science Division, Lawrence Berkeley Laboratory
University of California, Berkeley, California 94720

September 30, 1989

Abstract:

The mass fluctuations in damped reactions of $^{16}O + ^{16}O$ are studied in an extended time-dependent Hartree-Fock theory. The theory determines the time evolution of a two-body density matrix as well as that of a one-body density matrix, providing us with a microscopic way to calculate the fluctuations of one-body quantities. The results of the theory are compared with those obtained in a transport model. It is found that the dispersions in fragment mass calculated in the two models are of the same order of magnitude and much larger than those calculated in the time-dependent Hartree-Fock theory. The differences between the microscopic theory and the transport model are also discussed.

PACS numbers: 24.10.Cn, 25.70.Cd

*This work was supported by the National Science Foundation and the Director, Office of Energy Research, Office of High Energy and Nuclear Physics, Division of High Energy Physics, of the U.S. Department of Energy under Contract No. DE-AC03-76SF00098.

1 Introduction

A characteristic aspect of damped nuclear reactions is the broad distribution of the observables such as mass, charge, energy and angular momentum[1]. The most fundamental theory so far applied to damped reactions is the time-dependent Hartree-Fock (*TDHF*) theory.[2,3] Although the mean values of one-body observables are rather well reproduced by the *TDHF* model, the calculated fluctuations have been found to be significantly too small. For example, the mass dispersions calculated in *TDHF* for heavy systems are one order of magnitude smaller than experimental data.[3] This failure arises from the one-body nature of *TDHF*: the total wave function in *TDHF* is restricted to a single Slater determinant which is inadequate for the evaluation of expectation values of two-body operators, e.g. dispersions of one-body quantities.[4] Some microscopic approaches have been proposed to treat the fluctuations better. For example, Yamaji and Tohyama included two-particle-two-hole configurations in a perturbative way.[5] They found that the mass dispersions in $^{16}O + ^{40}Ca$ are enhanced by a factor of three as compared to *TDHF* results. However, the effects of nucleon-nucleon (*NN*) collisions on the dynamics of the heavy-ion collision are neglected in their approach. A different approach taken by Bonche and Flocard[6] and Marston and Koonin[7] are based on the variation principle proposed by Balian and Véneroni[8] which provides a method for calculating the fluctuations in the framework of a mean-field theory. The numerical results for $^{16}O + ^{16}O$ and $^{40}Ca + ^{40}Ca$ showed a $30 - 400\%$ increase in the mass dispersions. However, the effect of *NN* collisions on the dynamical development of the system are not included in this approach either.

In part I of this series of papers,[9] we developed a new, consistent method for calculating fluctuations. This method, called the time-dependent density-matrix theory (*TDDM*), was derived from the time-dependent density-matrix formalism proposed by Wang and Cassing[10] which includes the effects of *NN* collisions. *TDDM* determines the time evolution of the two-body density matrix in addition to that of the one-body density matrix. In ref. 9 we applied the *TDDM* to the damping of the isoscalar quadrupole motions of ^{16}O and ^{40}Ca and found that *TDDM* gives decay widths comparable to the experimental values.

In the present paper we apply the *TDDM* to the partition of mass in damped reactions. Since *TDDM* provides the two-body density matrix, as well as the one-body density matrix, it is straightforward to calculate the fluctuations of one-body observables. The aim of the paper is then to ascertain whether *TDDM* gives sufficiently large fluctuations in mass asymmetry to eliminate the qualitative failure of *TDHF*.

We focus on the reaction $^{16}O + ^{16}O$ which is the largest system we can practically treat for the present. Since no experimental data are available on the mass dispersions in $^{16}O + ^{16}O$, we compare our results with those calculated in a transport theory called the nucleon exchange transport model (*NET*)[11,12,13]. *NET* has been successful in reproducing experiment data for various systems[1]. Therefore, the results in *NET* for $^{16}O + ^{16}O$ are considered to be "empirical" values. In the comparison between *NET* and *TDDM*, basic macroscopic parameters in *NET* are obtained from quantities calculated in *TDDM*.

The presentation is organized as follows. A brief description of *TDDM* and *NET*

is given in Sect. 2, and important details of numerical calculations are explained in Sect. 3. The results on $^{16}O + ^{16}O$ are then presented in Sect. 4, while Sect. 5 is devoted to a summary.

2 Formalism

In this section we briefly describe the two models employed.

2.1 Time-dependent density-matrix theory

The *TDDM* treatment was formulated on the basis of the density-matrix formalism of Wang and Cassing.[10] Since the derivation was discussed in ref. 9 and ref. 14, we show only the basic equations of *TDDM*. The density matrix formalism[10] determines the time evolution of the one-body density matrix ρ and the correlated part of the two-body density matrix $C_2 = \rho_2 - \mathcal{A}(\rho\rho)$, where the second term is the antisymmetrized product of the one-body density matrices. We expand ρ and C_2 on a finite number of single-particle states $\{\psi_\lambda\}$:

$$\rho(11';t) = \sum_{\alpha,\beta} n_{\alpha\beta}(t)\ \psi_\alpha(1,t)\ \psi^*_\beta(1',t)\ , \tag{1}$$

$$C_2(12,1'2';t) = \sum_{\alpha\beta\alpha'\beta'} C_{\alpha\beta\alpha'\beta'}(t)\ \psi_\alpha(1,t)\ \psi_\beta(2,t)\ \psi^*_{\alpha'}(1',t)\ \psi^*_{\beta'}(2',t)\ , \tag{2}$$

where the numbers denote space, spin, and isospin coordinates. The time evolution of ρ and C_2 is determined by the following three equations. The first equation gives the single-particle representation:

$$i\hbar\dot{\psi}_\lambda(1,t) = h\psi_\lambda(1,t) = \left[-\hbar^2\frac{\nabla^2}{2M} + U[\rho]\right]\psi_\lambda(1,t)\ , \tag{3}$$

where the mean field $U[\rho]$ is defined as

$$U[\rho]\psi_\lambda(1,t) = \int d2\{v(12)[\rho(22;t)\psi_\lambda(1,t) - \rho(12;t)\psi_\lambda(2,t)]\}\ . \tag{4}$$

Here $v(12)$ is the effective interaction. The occupation matrix $n_{\alpha\beta}$ satisfies

$$i\hbar\dot{n}_{\alpha\beta} = \sum_{\gamma\delta\sigma}\{C_{\gamma\delta\beta\sigma} < \alpha\sigma|v|\gamma\delta > -C_{\alpha\delta\gamma\sigma} < \gamma\sigma|v|\beta\delta >\}\ . \tag{5}$$

The third equation determines the time evolution of $C_{\alpha\beta\alpha'\beta'}$,

$$i\hbar\dot{C}_{\alpha\beta\alpha'\beta'} = B_{\alpha\beta\alpha'\beta'}(t) + H_{\alpha\beta\alpha'\beta'}(t) + P_{\alpha\beta\alpha'\beta'}(t)\ , \tag{6}$$

where B is the lowest-order contribution with respect to $v(12)$, i.e. the Born term, and H and P contain terms describing particle-hole and particle-particle correlations to infinite order. The explicit expressions of B, H and P are given in the Appendix.

The three coupled equations (3), (5), and (6) satisfy conservation of total nucleon number, energy, and momentum (both linear and angular), and parity.[9,10]

In damped reactions the system maintains a binary character throughout and, in particular, there are two fragments in the final state of the collision. In order to count the number of nucleons in one of the fragments, we introduce the operator N_R

$$N_R = \int_R d\mathbf{r}\; a^\dagger(\mathbf{r})\; a(\mathbf{r})\;, \tag{7}$$

where $a^\dagger(\mathbf{r})$ and $a(\mathbf{r})$ are the creation and annihilation operators, respectively, and the subscript R means that the integration is restricted to half space containing one of the two fragments.[3] The mean nucleon number of one fragment is given by the expectation value of the operator:

$$< N_R >= \int_R d\mathbf{r}\; \rho(\mathbf{r},\mathbf{r})\;. \tag{8}$$

The variance of the mass distribution,

$$\sigma_R^2 =< N_R^2 > - < N_R >^2\;, \tag{9}$$

involves the two-body operator (the first term on the right-hand side). Therefore, it is given in terms of both the one-body and two-body density matrices:

$$\begin{aligned}\sigma_R^2 &= \int_R d\mathbf{r}\; \rho(\mathbf{r};\mathbf{r}) - \int_R d\mathbf{r}_1 d\mathbf{r}_2\; \rho(\mathbf{r}_1;\mathbf{r}_2)\; \rho(\mathbf{r}_2;\mathbf{r}_1) \\ &+ \int_R d\mathbf{r}_1 d\mathbf{r}_2\; c_2(\mathbf{r}_1\mathbf{r}_2;\mathbf{r}_1\mathbf{r}_2)\;.\end{aligned} \tag{10}$$

Eq. (10) can be written in terms of $n_{\alpha\beta}$ and $C_{\alpha\beta\alpha'\beta'}$

$$\begin{aligned}\sigma_R^2 &= \sum_{\alpha\beta} n_{\alpha\beta} < \beta|\alpha >_R \\ &+ \sum_{\alpha\beta\alpha'\beta'} < \alpha'|\alpha >_R < \beta'|\beta >_R \left(C_{\alpha\beta\alpha'\beta'} - n_{\alpha\beta'} n_{\beta\alpha'}\right)\;,\end{aligned} \tag{11}$$

where $< \alpha|\beta >_R$ is the overlap integral of the two single-particle states α and β in the half space. Since $n_{\alpha\beta} = \delta_{\alpha\beta}$ and $C_{\alpha\beta\alpha'\beta'} = 0$ in *TDHF* , σ_R in *TDHF* simplifies

$$\sigma_{RTDHF}^2 = \sum_{\lambda=1}^{A} < \lambda|\lambda >_R \; - \sum_{\lambda,\lambda'}^{A} < \lambda|\lambda' >_R < \lambda'|\lambda >_R\;, \tag{12}$$

where A is the total number of nucleons.

Since the total system is an eigenstate of the total number operator, the dispersion for the entire space must be zero

$$\begin{aligned}\sigma_{\text{total}}^2 &= \sum_{\alpha} n_{\alpha\alpha} + \sum_{\alpha\beta}(C_{\alpha\beta\alpha\beta} - n_{\alpha\beta} n_{\beta\alpha}) \\ &= A + \sum_{\alpha\beta}(C_{\alpha\beta\alpha\beta} - n_{\alpha\beta} n_{\beta\alpha}) \;=\; 0\;.\end{aligned} \tag{13}$$

where $< \alpha|\beta >_{\text{total}} = \delta_{\alpha\beta}$ has been used. *TDHF* conserves this condition because $C_{\alpha\beta\delta\gamma} = 0$ and $n_{\alpha\beta} = \delta_{\alpha\beta}$. In Appendix it is shown that *TDDM* also satisfies the above condition. As is discussed in Appendix, the Born approximation for $C_{\alpha\beta\alpha'\beta'}$ does not satisfy the condition (Eq. 13). The higher-order terms must be included to satisfy the condition that the system is an eigenstate of the number operator.

2.2 Nucleon exchange transport model

In this subsection we briefly present how to calculate the mass dispersions in *NET*. The details of *NET* are presented in refs. 11-13. The *NET* formulas presented below contain the macroscopic variables A and B which are the mass numbers of the two reaction partners. Since the total mass number is conserved, A may be chosen as the independent macroscopic variable. The time derivative of the mass variance in *NET* is given by[13]

$$\frac{d}{dt}\sigma_A^2 \;=\; 2D_{AA} \;+\; 2\,\frac{\partial V_A}{\partial A}\,\sigma_A^2\;, \tag{14}$$

where D_{AA} is the mass diffusion coefficient and V_A the mass drift coefficient. The diffusion coefficient is evaluated under the assumption that the two nuclei are Fermi gases with the same temperature τ. D_{AA} is then given by

$$D_{AA} \;=\; \frac{n_0}{T_F}\,\pi c_{\rm eff}^2\,\tau^*, \tag{15}$$

where $c_{\rm eff}(t)$ is the time-dependent effective neck radius. $T_F \approx 37$ MeV denotes the Fermi kinetic energy and $n_0 \approx 2.5 \times 10^{21}$ fm^{-2}s^{-1} is the one-way nucleon flux in standard nuclear matter.[13] Furthermore, the "effective temperature" τ^* is given by

$$\tau^* \;=\; \frac{\omega_{\rm eff}}{2}\,\coth\frac{\omega_{\rm eff}}{2\tau}\;, \tag{16}$$

where τ is obtained from the dissipated collective energy Q using the relation $Q = (A+B)\tau^2/(8\ \text{MeV})$. The effective excitation energy $\omega_{\rm eff}$ is given by $\omega_{\rm eff}^2 = \frac{1}{2}P_F^2(\dot{R}^2 + U_t^2)$, where $\dot{R}$ is the radial velocity, u_t is the tangential velocity, and $P_F = 265$ MeV/c is the Fermi momentum in standard nuclear matter. In the calculations for ^{16}O + ^{16}O we use a rotational-frame approximation for peripheral collisions. In this approximation U_t =0. The drift coefficient depends on the potential energy of the dinucleus and is obtained from the Lysekil mass formula.[15] Its derivative is then given by[13],

$$\begin{aligned}\frac{\partial V_A}{\partial A} \;=\; & \frac{2n_0}{T_f}\pi c_{\rm eff}^2\Big[-\frac{m}{2A}(\dot{R}^2+\omega^2R^2) \\ & +\frac{m}{9A}R^2\omega^2 + \frac{4}{9}a_2A^{-\frac{4}{3}} - \frac{5}{9}c_3A^{-\frac{1}{3}} + \frac{2}{A^2}V_{\rm c}\Big]\;,\end{aligned} \tag{17}$$

where the Coulomb energy is

$$V_{\rm c} \;=\; \begin{cases} e^2\frac{A^2}{4R_0}(2-\frac{R}{R_0})\;, & R \le R_0 \\ e^2\frac{A^2}{4R}\;, & R \ge R_0 \end{cases} \tag{18}$$

Here R is the distance between the two nuclear centers, R_0 the sum of the nuclear radii, ω the rotational frequency, and the liquid-drop coefficients are $a_2 = 17.9437$ MeV and $c_3 = 0.7053$ MeV. The time evolution of the quantities $c_{\rm eff}$, τ^*, R, $\dot{R}$, and ω is calculated in *TDDM*.†

†We wish to note that in ref. 13 there is a typographical error in the expression for the restoring force: in (A.31) the mixed derivative (first line) is missing the (relatively small) Coulomb term $\frac{2}{3}(Z_A/A^{4/3} + Z_B/B^{4/3})c_3$, although this term *was* included in the associated *NET* computer code.

3 Calculational details

Employing the two models described above, we have studied the reaction ^{16}O +^{16} O at a bombarding energy of 185 MeV. The numerical procedures for solving the coupled equations of *TDDM* are similar to those used in part I of this series,[9] so we only note a few points specific to ^{16}O +^{16} O. Eq. (3) for the single-particle wave functions is solved using a *TDHF* code with axial symmetry.[16] The initial single-particle wave functions are boosted with the phase factor associated with the relative motion of the two nuclei. For collisions at finite impact parameters the single-particle wave functions are calculated in a rotating frame. The *TDHF* code uses several prescriptions for the calculation of the moment of inertia. We employ the so-called *R4* prescription[17] because it produces a moment of inertia that changes continuously with time and, therefore, leads to a smooth time dependence of the extracted temperature τ. Furthermore, our calculation incorporates the single-particle orbitals through to the $2s - 1d$ shell (with the $1s$ and $1p$ orbitals being occupied initially). We use a simple residual interaction of the δ-function form, $v = v_0\delta^3(\mathbf{r} - \mathbf{r}')$ with $v_0 = -300$ MeV fm^3. The strength of the residual interaction appears to be reasonable because the damping widths of the isoscalar quadrupole resonances of ^{16}O and ^{40}Ca were reproduced with this residual interaction.[9]

The time-dependent quantities entering in the *NET* model, i.e. the separation R, its time derivative $\dot{R}$ (the radial velocity), the effective neck radius $c_{\rm eff}$, and the angular frequency ω are calculated on the basis of the density distribution obtained in the *TDDM* model, at each time step.[16,18] This latter quantity is determined from the relation $\omega = L/\mathcal{I}(\rho)$, where L is the angular momentum and $\mathcal{I}(\rho)$ is the moment of inertia. Following the prescription developed in ref. 18, we determine the effective neck radius $c_{\rm eff}$ from the one-way current

$$N = n_0\pi c_{\rm eff}^2 = n_0 \int_{\rm window} dxdy \left(\frac{\rho(x,y,z=0)}{\rho_0}\right)^{4/3} , \qquad (19)$$

where N is the total transfer current across the neck, $\rho_0 = 0.17$ fm^{-3} is the nuclear matter density. At each time step, the nuclear temperature τ is determined from the total kinetic energy loss obtained in the *TDDM* calculation.

4 Results

We first sought to determine the fusion threshold, i.e. that incident energy above which fusion no longer occurs for a head-on collision, and found it to be $E_{\rm lab} \approx 170$ MeV. This value is considerably higher than that obtained in *TDHF* which is only 54 MeV when the spin-orbit force is not included. However, it is not so high as the result ($E_{\rm lab} \approx 140$ MeV) of the previous *TDDM* calculation[19] which included only the Born term in Eq. (6). This indicates that the higher-order terms in Eq. (6) are not as important as the Born term, as far as the dissipation in nuclear collisions is concerned. The effects of the higher-order correlations in Eq. (6) were also studied by Cassing and Wang for a one-dimensional system.[20] Solving the coupled equations for ρ and

C_2 in coordinate space using a bare NN interaction with a short range repulsive part, they found that the dissipation due to the NN collisions is weakened by the higher-order terms. Their finding is apparently inconsistent with our result. We interpret the difference in the following way. The higher-order terms may play two different roles: one is to renormalize the bare NN interaction and the other modify the phase-space distribution of two nucleons. The calculation by Cassing and Wang[20] has no truncation in momentum space, since the coupled equations were solved in coordinate space. Therefore, it is likely that they observed the drastic renormalization of the bare interaction when they included the higher-order terms. We believe that this renormalization effect is small in our calculation because of the severe truncation in single-particle space. There still remains the effect of modification of the phase-space distribution due to the higher-order correlations. This effect enhances the dissipation, as was found in the damping of giant resonances.[9]

We calculate the mass dispersions for two different reactions, namely a head-on collision and a peripheral collision ($L = 40\hbar$) at $E_{\rm lab} = 185$ MeV. The incident energy is chosen to be above the determined fusion threshold. In table 1 we show the loss in kinetic energy of relative motion and the reaction times, as calculated in *TDHF* and *TDDM*. The reaction time is defined as the period during which two nuclei are clutched[16] (i.e. the density in the middle of the neck exceeds half of the nuclear matter density). *TDDM* gives larger kinetic energy losses and longer reaction times than *TDHF*. However, in the head-on collision effect of the two-body collisions is relatively small.

The change in the occupation matrix may be described by the entropy defined by[21]

$$S = -\sum_{\alpha}\{n_\alpha \ln n_\alpha + (1-n_\alpha)\ln(1-n_\alpha)\} \ , \qquad (20)$$

where $\{n_\alpha\}$ is the eigenvalues of the occupation matrix. This quantity is shown in Fig. 1 as a function of time. The entropy increases rapidly in the initial stage of the collision and reaches a steady value at the final stage. The asymptotic values for the head-on and peripheral collisions are about $36k_B$ and $18k_B$, respectively. Using the temperatures obtained in the *NET* calculation, which are shown in Fig. 2–3, the Fermi-gas model gives entropies of $39k_B$ for the head-on collision and $23k_B$ for the peripheral collision.

The time evolution of the quantities needed in the transport equation for the mass dispersion are shown in Figs. 2–3 (τ and τ^*) and Fig. 4 (D_{AA}). Although *NET* is developed to treat reactions with relatively small overlap between the two nuclei, such as occurs for our peripheral case, we also employ it for the head-on collision in order to estimate the order of magnitude of the mass dispersion. The increase in the effective temperature in the final stage of the peripheral reaction is due to the increase in $\dot{R}$. The effective temperature approaches an asymptotic value as the two fragments separate. The peak in τ^* in the head-on collision is due to an increase in the collective energy after many nucleons from one nucleus penetrate into the other nucleus. The temporal behavior of D_{AA} is mainly determined by the one-way current N (Eq. (19)) which is plotted in Fig. 5 with solid curves. The double peaks of D_{AA} seen in the head-on collision is caused by peak of the effective temperature (see Fig. 2). In the case

3 Calculational details

Employing the two models described above, we have studied the reaction $^{16}O + ^{16}O$ at a bombarding energy of 185 MeV. The numerical procedures for solving the coupled equations of *TDDM* are similar to those used in part I of this series,[9] so we only note a few points specific to $^{16}O + ^{16}O$. Eq. (3) for the single-particle wave functions is solved using a *TDHF* code with axial symmetry.[16] The initial single-particle wave functions are boosted with the phase factor associated with the relative motion of the two nuclei. For collisions at finite impact parameters the single-particle wave functions are calculated in a rotating frame. The *TDHF* code uses several prescriptions for the calculation of the moment of inertia. We employ the so-called *R4* prescription[17] because it produces a moment of inertia that changes continuously with time and, therefore, leads to a smooth time dependence of the extracted temperature τ. Furthermore, our calculation incorporates the single-particle orbitals through to the $2s - 1d$ shell (with the $1s$ and $1p$ orbitals being occupied initially). We use a simple residual interaction of the δ-function form, $v = v_0\delta^3(\mathbf{r} - \mathbf{r}')$ with $v_0 = -300$ MeV fm^3. The strength of the residual interaction appears to be reasonable because the damping widths of the isoscalar quadrupole resonances of ^{16}O and ^{40}Ca were reproduced with this residual interaction.[9]

The time-dependent quantities entering in the *NET* model, i.e. the separation R, its time derivative $\dot{R}$ (the radial velocity), the effective neck radius $c_{\rm eff}$, and the angular frequency ω are calculated on the basis of the density distribution obtained in the *TDDM* model, at each time step.[16,18] This latter quantity is determined from the relation $\omega = L/\mathcal{I}(\rho)$, where L is the angular momentum and $\mathcal{I}(\rho)$ is the moment of inertia. Following the prescription developed in ref. 18, we determine the effective neck radius $c_{\rm eff}$ from the one-way current

$$N = n_0\pi c_{\rm eff}^2 = n_0 \int_{\rm window} dxdy \left(\frac{\rho(x,y,z=0)}{\rho_0}\right)^{4/3} , \qquad (19)$$

where N is the total transfer current across the neck, $\rho_0 = 0.17$ fm^{-3} is the nuclear matter density. At each time step, the nuclear temperature τ is determined from the total kinetic energy loss obtained in the *TDDM* calculation.

4 Results

We first sought to determine the fusion threshold, i.e. that incident energy above which fusion no longer occurs for a head-on collision, and found it to be $E_{\rm lab} \approx 170$ MeV. This value is considerably higher than that obtained in *TDHF* which is only 54 MeV when the spin-orbit force is not included. However, it is not so high as the result ($E_{\rm lab} \approx 140$ MeV) of the previous *TDDM* calculation[19] which included only the Born term in Eq. (6). This indicates that the higher-order terms in Eq. (6) are not as important as the Born term, as far as the dissipation in nuclear collisions is concerned. The effects of the higher-order correlations in Eq. (6) were also studied by Cassing and Wang for a one-dimensional system.[20] Solving the coupled equations for ρ and

C_2 in coordinate space using a bare NN interaction with a short range repulsive part, they found that the dissipation due to the NN collisions is weakened by the higher-order terms. Their finding is apparently inconsistent with our result. We interpret the difference in the following way. The higher-order terms may play two different roles: one is to renormalize the bare NN interaction and the other modify the phase-space distribution of two nucleons. The calculation by Cassing and Wang[20] has no truncation in momentum space, since the coupled equations were solved in coordinate space. Therefore, it is likely that they observed the drastic renormalization of the bare interaction when they included the higher-order terms. We believe that this renormalization effect is small in our calculation because of the severe truncation in single-particle space. There still remains the effect of modification of the phase-space distribution due to the higher-order correlations. This effect enhances the dissipation, as was found in the damping of giant resonances.[9]

We calculate the mass dispersions for two different reactions, namely a head-on collision and a peripheral collision ($L = 40\hbar$) at $E_{\rm lab} = 185$ MeV. The incident energy is chosen to be above the determined fusion threshold. In table 1 we show the loss in kinetic energy of relative motion and the reaction times, as calculated in *TDHF* and *TDDM*. The reaction time is defined as the period during which two nuclei are clutched[16] (i.e. the density in the middle of the neck exceeds half of the nuclear matter density). *TDDM* gives larger kinetic energy losses and longer reaction times than *TDHF*. However, in the head-on collision effect of the two-body collisions is relatively small.

The change in the occupation matrix may be described by the entropy defined by[21]

$$S = -\sum_{\alpha}\{n_\alpha \ln n_\alpha + (1-n_\alpha)\ln(1-n_\alpha)\} \ , \tag{20}$$

where $\{n_\alpha\}$ is the eigenvalues of the occupation matrix. This quantity is shown in Fig. 1 as a function of time. The entropy increases rapidly in the initial stage of the collision and reaches a steady value at the final stage. The asymptotic values for the head-on and peripheral collisions are about $36k_B$ and $18k_B$, respectively. Using the temperatures obtained in the *NET* calculation, which are shown in Fig. 2–3, the Fermi-gas model gives entropies of $39k_B$ for the head-on collision and $23k_B$ for the peripheral collision.

The time evolution of the quantities needed in the transport equation for the mass dispersion are shown in Figs. 2–3 (τ and τ^*) and Fig. 4 (D_{AA}). Although *NET* is developed to treat reactions with relatively small overlap between the two nuclei, such as occurs for our peripheral case, we also employ it for the head-on collision in order to estimate the order of magnitude of the mass dispersion. The increase in the effective temperature in the final stage of the peripheral reaction is due to the increase in $\dot{R}$. The effective temperature approaches an asymptotic value as the two fragments separate. The peak in τ^* in the head-on collision is due to an increase in the collective energy after many nucleons from one nucleus penetrate into the other nucleus. The temporal behavior of D_{AA} is mainly determined by the one-way current N (Eq. (19)) which is plotted in Fig. 5 with solid curves. The double peaks of D_{AA} seen in the head-on collision is caused by peak of the effective temperature (see Fig. 2). In the case

of peripheral collision the average value of D_{AA} over the reaction time is $2 \cdot 10^{21}$ s^{-1}. This value is close to the "empirical" value D $\approx (A+B) \cdot 10^{20}$ s^{-1} $= 32 \cdot 10^{20}$ s^{-1} which is used in a simple transport model[22].

The time evolution of the mass dispersions calculated in *TDDM* (Eq. (11)), *TDHF* (Eq. (12)) and *NET* are plotted in Fig. 6. The mass dispersions in *NET* are dominated by the diffusion term (the first term on the right hand side of Eq. (14)). All the results of the mass dispersion are quite stable as functions of time after the two ions are well separated. The entire space integral of Eq. (13) was calculated to check numerical accuracy and was found to be smaller than 0.02. The final-state mass dispersions in *TDDM*, *TDHF* and *NET* are shown in table 2. The *TDDM* results are of the same order of magnitude as the *NET* values, whereas *TDHF* results are much smaller. Since *NET* values are considered as "empirical", the final-state *TDDM* results may be large enough to reproduce experimental mass fluctuations.

There is a noticeable difference between the *TDDM* results and the *NET* ones in the intermediate stage of the collisions. While the transport model yields a monotonically increasing mass variance, the quantal results exhibit large peaks at early times, before approaching their respective final values. Before discussing this difference we look at the mass dispersions in *TDDM* in more detail.

We separate the expression for σ_R^2 (Eq. (11)) into two parts corresponding to a one-body contribution and a two-body correlation contribution,

$$\sigma_R^2 = \sum_{\alpha\beta} n_{\alpha\beta} < \beta|\alpha >_R - \sum_{\alpha\beta\alpha'\beta'} < \alpha'|\alpha >_R < \beta'|\beta >_R n_{\alpha\beta'} n_{\beta\alpha'} \qquad (21)$$

$$+ \sum_{\alpha\beta\alpha'\beta'} < \alpha'|\alpha >_R < \beta'|\beta >_R C_{\alpha\beta\alpha'\beta'} \, . \qquad (22)$$

Each contribution is separately shown in Fig. 7. The time when the one-body and two-body contributions start growing is the time when the NN collisions were turned on. This time is slightly before the two nuclei start overlapping. The non-zero contribution from each part before the collision of the two nuclei is due to the ground-state correlations. The sum of these contributions is equal to zero before the two nuclei overlap, guaranteeing that each nucleus is an eigenstate of the number operator.

For the head-on collision the two-body contribution has a sharp peak (see Fig. 7) which is not seen in the peripheral collision. The peak arises from an increase in the two-body correlation matrix as a result of a decrease in the energy gap between the occupied and unoccupied single-particle states. Fig. 8 shows the time evolution of some of the single-particle energies defined by $\epsilon_\lambda =< \lambda|h|\lambda >$. The energy gap between the $1p$ state and the $2d$ state becomes very small when the two nuclei overlap strongly. Therefore, the dominant two-body correlation matrix in the initial stage of the collision, i.e. the two-particle two-hole matrix (which is inversely proportional to the energy gap), is enhanced when the energy gap becomes small.

In the transport treatment, the growth of the mass variance is driven by the directed current of transferred nucleons N, given in Eq. (19). In order to understand the decrease in the *TDDM* mass variance during the final stage of the reaction, we

introduce a corresponding directed current[18]

$$N = \int dxdy\ J_z^{A\to B}(z=0)\ . \tag{23}$$

where $J_z^{A\to B}$ is the z component (beam direction) of the current density associated with the orbitals originally in nucleus A,

$$\mathbf{J}^{A\to B}(\mathbf{r}) = \sum_{\alpha\beta} n_{\alpha\beta}\ \frac{i\hbar}{2m}\{\psi_\alpha \nabla\psi_\beta^* - \psi_\beta^* \nabla\psi_\alpha\}\ . \tag{24}$$

The sum in the above expression includes those single-particle orbitals that were initially localized in nucleus A. Of course, the directed current thus defined has no direct physical significance, since the single-particle orbitals become delocalized when the two nuclei start to overlap. The directed current (23) is plotted in Fig. 5 with dashed curves. The current in *TDDM* is not positive definite and becomes negative in the later stage of the collision. Using Eq. (23), we calculated the mass dispersions in *NET*. The results are shown in Fig. 9 with dashed curves. The temporal behavior of the mass dispersion is now similar to the *TDDM* result i.e. the decrease of σ_R^2 toward the final state. The above qualitative discussion suggests that the discrepancy between *TDDM* and *NET* originates in the assumption of quick memory loss inherent in the transport treatment. For central collisions of relatively small nuclei, the opportunity for the single-particle motion to become disordered is significantly reduced and the transferred particles may remain coherent beyond the echo time and thus reduce the mass variance when transferred back to their original host nucleus. Clearly, the time local treatment of the *NET* model is inadequate for such a situation.

In the following we point out some ambiguities in our calculation. The initial Hartree-Fock ground state is not the true ground state of *TDDM* as was discussed in ref. 9. Since the ground state correlations grow in time, the mass dispersions may depend on when the *NN* collisions are switched on. For the head-on collision we made two calculations with different starting time of the *NN* collisions; in one calculation the *NN* collisions are turned on when the separation distance of the two nuclei is 5.2 fm and in the other the distance is 9 fm. The former has practically no ground state correlations grown before the two nuclei overlap, and the latter fully grown correlations. It was found that σ_R^2 vary from 3.6 to 4.0 when the separation distance changes from 5.2 fm to 9 fm. The mass dispersions are, therefore, not very sensitive to the initial ground state correlations.

In the peripheral collisions the kinetic energy loss and the reaction time depend on how the moment of inertia is calculated. The *R4* prescription[17] which gives a continuous change in the moment of inertia was found to give a larger kinetic energy loss and a longer reaction time than other prescriptions, such as *R2*. As a result of the longer reaction time, the *R4* prescription gives a larger mass dispersion than *R2*.

The total energy for the head-on collision is shown in Fig. 10 as a function of time. Although the equations of motion Eq. (3) – (6) formally satisfy energy conservation, the total energy is not conserved in our numerical calculation, as was found in our previous calculations[9,19]. Some gain in energy occurs during the time when the two

nuclei strongly overlap. The violation of the energy conservation is not sensitive to the change in the parameters in the numerical calculations, such as the number of mesh points and mesh sizes. Therefore we conclude that the violation is mainly due to the truncation in the single-particle space, as was discussed in ref. 9.

We also calculated the relative momentum dispersion, as was done in ref. 7. Since the initial Hartree-Fock state is not an eigenstate of the relative momentum operator, the initial dispersion of the momentum is finite, $\sigma_P = 1.17$ fm^{-1}. We found a slight increase in the momentum dispersion in the final state. However, it is of the same order of magnitude as the *TDHF* result. This suggests that a reliable calculation of the momentum dispersion may require the inclusion of the fluctuations in the mean field, an effect that has so far not been considered.

5 Summary

We studied the mass dispersions in damped reactions of $^{16}O + ^{16}O$ at $E_{lab} = 185$ MeV, based on the time-dependent density matrix theory. The advantage of the *TDDM* theory is that it provides the two-body density matrix determined consistently with the dynamics of a nuclear reaction. The fluctuations of one-body observables, such as fragment mass, were calculated with the two-body density matrix. It was found that the mass dispersions calculated in *TDDM* are considerably larger than those in *TDHF*, by factors of 2.5–3. The *TDDM* results were also compared with the nucleon exchange transport model which reproduces experimental data for many reaction systems. The *TDDM* results were of the same order of magnitude as those of the *NET* model. We have also discussed the difference in the temporal behavior of the mass dispersion between *TDDM* and *NET* and it was noted that the *NET* assumption of quick internal relaxation is not satisfactory for an accurate description of the dynamics of these nuclear reaction processes.

Acknowledgment

This work was supported by the National Science Foundation and by the Director, Office of High Energy and Nuclear Physics of the Department of Energy under contract DE-AC03-76SF00098.

A Number conservation

In this appendix we prove that *TDDM* satisfies the number-conservation condition Eq. (13). For that we use the explicit expression for the equation of motion for $C_{\alpha\beta\alpha'\beta'}$,

$$i\hbar\dot{C}_{\alpha\beta\alpha'\beta'} = B_{\alpha\beta\alpha'\beta'}(t) + H_{\alpha\beta\alpha'\beta'}(t) + P_{\alpha\beta\alpha'\beta'}(t) \ ,$$

where

$$\begin{aligned}
B_{\alpha\beta\alpha'\beta'} &= \sum_{\lambda_1\lambda_2\lambda_3\lambda_4} < \lambda_1\lambda_2|v|\lambda_3\lambda_4 >_a \\
&\{(\delta_{\alpha\lambda_1} - n_{\alpha\lambda_1})(\delta_{\beta\lambda_2} - n_{\beta\lambda_2})n_{\lambda_3\alpha'}n_{\lambda_4\beta'} \\
&-n_{\alpha\lambda_1}n_{\beta\lambda_2}(\delta_{\lambda_3\alpha'} - n_{\lambda_3\alpha'})(\delta_{\lambda_4\beta'} - n_{\lambda_4\beta'})\} \ , \qquad (25) \\
H_{\alpha\beta\alpha'\beta'} &= \sum_{\lambda_1\lambda_2\lambda_3\lambda_4} < \lambda_1\lambda_2|v|\lambda_3\lambda_4 > \\
&\{\delta_{\alpha\lambda_1}(n_{\lambda_3\alpha'}C_{\beta\lambda_4\beta'\lambda_2} - n_{\lambda_3\beta'}C_{\beta\lambda_4\alpha'\lambda_2} \\
&\quad - n_{\lambda_4\alpha'}C_{\lambda_3\beta\lambda_2\beta'} - n_{\lambda_4\beta'}C_{\lambda_3\beta\alpha'\lambda_2}) \\
&+\delta_{\beta\lambda_2}(n_{\lambda_4\beta'}C_{\alpha\lambda_3\alpha'\lambda_1} - n_{\lambda_4\alpha'}C_{\alpha\lambda_3\beta'\lambda_1} \\
&\quad - n_{\lambda_3\beta'}C_{\alpha\lambda_4\alpha'\lambda_1} - n_{\lambda_3\alpha'}C_{\alpha\lambda_4\lambda_1\beta'}) \\
&-\delta_{\lambda_3\alpha'}(n_{\alpha\lambda_1}C_{\beta\lambda_4\beta'\lambda_2} - n_{\beta\lambda_1}C_{\alpha\lambda_4\beta'\lambda_2} \\
&\quad - n_{\alpha\lambda_2}C_{\beta\lambda_4\beta'\lambda_1} - n_{\beta\lambda_2}C_{\alpha\lambda_4\lambda_1\beta'}) \\
&-\delta_{\lambda_4\beta'}(n_{\beta\lambda_2}C_{\alpha\lambda_3\alpha'\lambda_1} - n_{\alpha\lambda_2}C_{\beta\lambda_3\alpha'\lambda_1} \\
&\quad - n_{\beta\lambda_1}C_{\alpha\lambda_3\alpha'\lambda_2} - n_{\alpha\lambda_1}C_{\beta\lambda_3\lambda_2\alpha'})\} \ , \qquad (26) \\
P_{\alpha\beta\alpha'\beta'} &= \sum_{\lambda_1\lambda_2\lambda_3\lambda_4} < \lambda_1\lambda_2|v|\lambda_3\lambda_4 > \\
&\{\delta_{\alpha\lambda_1}\delta_{\beta\lambda_2}C_{\lambda_3\lambda_4\alpha'\beta'} - C_{\alpha\beta\lambda_1\lambda_2}\delta_{\lambda_3\alpha'}\delta_{\lambda_4\beta'} \\
&-\delta_{\alpha\lambda_1}n_{\beta\lambda_2}C_{\lambda_3\lambda_4\alpha'\beta'} - \delta_{\beta\lambda_2}n_{\alpha\lambda_1}C_{\lambda_4\lambda_3\beta'\alpha'} \\
&+\delta_{\lambda_3\alpha'}n_{\lambda_4\beta'}C_{\alpha\beta\lambda_1\lambda_2} + \delta_{\lambda_4\beta'}n_{\lambda_3\alpha'}C_{\alpha\beta\lambda_1\lambda_2}\} \ . \qquad (27)
\end{aligned}$$

The subscript a in Eq. (25) means that the matrix is antisymmetrized.

The time derivative of $\sum_{\alpha\beta} C_{\alpha\beta\alpha\beta}$ consists of three terms as can be seen from Eq. (6). Using the fact that the matrix element of the interaction is antisymmetrized, it is straightforward to show that the Born terms do not contribute, $\sum_{\alpha\beta} B_{\alpha\beta\alpha\beta} = 0$. In the sum of the higher-order contributions H and P several terms cancel and the remaining terms yield

$$\begin{aligned}
\sum_{\alpha\beta} H_{\alpha\beta\alpha\beta} &= -2 \sum_{\alpha\beta\lambda_2\lambda_3\lambda_4} < \alpha\lambda_2|v|\lambda_3\lambda_4 >_a n_{\lambda_3\beta}C_{\beta\lambda_4\alpha\lambda_2} \\
&\quad +2 \sum_{\lambda_1\lambda_2\lambda_4\alpha\beta} < \lambda_1\lambda_2|v|\alpha\lambda_4 >_a n_{\beta\lambda_1}C_{\alpha\lambda_4\beta\lambda_2}
\end{aligned}$$

and

$$\sum_{\alpha\beta} P_{\alpha\beta\alpha\beta} = -2 \sum_{\alpha\beta\lambda_2\lambda_3\lambda_4} < \alpha\lambda_2|v|\lambda_3\lambda_4 > n_{\beta\lambda_2}C_{\lambda_3\lambda_4\alpha\beta}$$

$$+2 \sum_{\alpha\beta\lambda_1\lambda_2\lambda_4} < \lambda_1\lambda_2|v|\alpha\lambda_4 > n_{\lambda_4\beta} C_{\alpha\beta\lambda_1\lambda_2} \quad (28)$$

The derivative of the sum of C finally becomes

$$\begin{aligned} \frac{d}{dt}\sum_{\alpha\beta} C_{\alpha\beta\alpha\beta} &= \frac{2}{i\hbar}\sum_{all}(n_{\lambda_3\beta} < \alpha\lambda_2|v|\lambda_4\lambda_3 > C_{\beta\lambda_4\alpha\lambda_2} \\ &\quad + n_{\beta\lambda_1} < \lambda_1\lambda_2|v|\alpha\lambda_4 > C_{\alpha\lambda_4\beta\lambda_2}) \\ &= 2\sum_{\alpha\beta} n_{\alpha\beta}\dot{n}_{\beta\alpha} \\ &= \frac{d}{dt}\sum_{\alpha\beta} n_{\alpha\beta}n_{\beta\alpha} \ . \end{aligned} \quad (29)$$

From the first to the second line we have used the equation of motion for $n_{\alpha\beta}$ (Eq. (5)). Thus Eq. (13) is time-independent. Since $\sigma^2_{\text{total}} = 0$ initially, Eq. (13) is always satisfied. From the above discussion we found that whether the condition (13) is satisfied or not depends on the approximation for the equation of motion for $C_{\alpha\beta\gamma\delta}$. In the Born approximation we always have $\sum_{\alpha\beta}\dot{C}_{\alpha\beta\alpha\beta} = 0$ because of $\sum_{\alpha\beta} B_{\alpha\beta\alpha\beta} = 0$. Since the time derivative of $\sum_{\alpha\beta} n_{\alpha\beta}n_{\beta\alpha}$ is not always zero, the Born approximation does not conserve the condition (13).

References

[1] See for example, Wolfgang U. Schröder and John R. Huizenga, *Treaties on Heavy Ion Science*, Vol **2** (Plenum, New York, 1984).

[2] J. W. Negele, Rev. Mod. Phys. 54, 913 (1982).

[3] K. T. R. Davies, K. R. S. Devi, S. E. Koonin and M. R. Strayer, *Treaties on Heavy Ion Science*, Vol **3** (Plenum, New York, 1985).

[4] C. H. Dasso, T. Døssing and H. C. Pauli, Z. Phys. A289, 395 (1979).

[5] M. Tohyama and S. Yamaji, Phys. Lett. **123**B, 16 (1983). S. Yamaji and M. Tohyama, Phys. Lett. **147**B, 339 (1984).

[6] P. Bonche and H. Flocard, Nucl. Phys. A**437**, 189 (1985).

[7] J. B. Marston and S. E. Koonin, Phys. Rev. Lett. **54**, 1139 (1985).

[8] R. Balian and M. Véneroni, Phys. Rev. Lett. **47**, 1353 (1981).

[9] M. Gong and M. Tohyama, Subm. to Z. Phys. **A** (1989).

[10] S. J. Wang and W. Cassing, Ann. Phys. **159**, 328 (1985).

[11] J. Randrup, Nucl. Phys. **A307** 319 (1978).

[12] J. Randrup, Nucl. Phys. **A327** 490 (1979).

[13] J. Randrup, Nucl. Phys. **A383** 468 (1982).

[14] M. Tohyama and M. Gong, Z. Phys. **A**332, 269 (1989).

[15] W.D. Myers and W.J. Swiatecki, Ark. Fys. **36** (1967) 343.

[16] K. T. R. Davies and S. E. Koonin, Phys. Rev. C**23**, 2042 (1981).

[17] K. T. R. Davies, H. T. Feldmeier, H. Flocard and M. S. Weiss, Phys. Rev. C**18**, 2631 (1978).

[18] F. H. Jørgensen, T. Døssing, B. S. Nilsson and J. Randrup, Phys. Lett. **191**B, 323 (1987).

[19] M. Tohyama, Phys. Rev. C**36**, 187 (1987).

[20] W. Cassing and S. J. Wang, Z. Phys. A328, 423 (1987).

[21] H. Feldmeier and P. Buck, in Lecture notes in physics, vol. 171 (Springer, Berlin 1982) p. 384

[22] W. U. Schröder and J. R. Huizenga, Ann. Rev. Nucl. Sci. **27**, 465 (1977).

Table 1: Total kinetic-energy loss *TKEL* (MeV) and reaction time t_{react} (10^{-21} s).

	$L = 0\hbar$		$L = 40\hbar$	
	TKEL	t_{react}	*TKEL*	t_{react}
TDDM	82	0.43	37	0.54
TDHF	64	0.25	11	0.25

Table 2: Mass dispersion σ_A calculated in *TDHF*, *TDDM* and *NET*.

	σ_A	
	$L = 0\hbar$	$L = 40\hbar$
TDHF	0.8	0.4
TDDM	2.0	1.2
NET	2.7	1.5

Figure captions

Figure 1: Entropies calculated with Eq. (20) for the collisions of $^{16}O + ^{16}O$ at $E_{lab} =$ 185 MeV. The solid curve is for the head-on reaction while the dashed curve is for the peripheral case ($L = 40\hbar$).

Figure 2: The time dependence of the temperature τ (solid) and the effective temperature τ^* (dashed) as calculated in *NET* for the head-on reaction. The arrows indicate the time interval during which two nuclei are clutched.

Figure 3: Same as Fig. 2 but for the peripheral collision ($L = 40\hbar$).

Figure 4: Diffusion coefficients in *NET* as functions of time. The arrows indicate the time interval during which two nuclei are clutched.

Figure 5: One-way currents as functions of time. The solid curves are calculated with Eq. (19), and the dashed curves with Eq. (23).

Figure 6: σ_R^2 as a function of time. The solid curves are the results of *TDDM*, the dashed curves are those of *TDHF*, and the dot-dashed curves the results of *NET*.

Figure 7: σ_R^2 calculated with Eq. (21) (solid), Eq. (22) (dashed), and the sum of both (dot-dashed).

Figure 8: Single-particle energies $\varepsilon_\lambda = < \lambda | h | \lambda >$ as functions of time for the head-on reaction. The azimuthal quantum number is denoted by m and $+$ and $-$ denote the z-parity.

Figure 9: The mass dispersion calculated in *NET* with the current Eq. (19) (solid) and with the current Eq. (23) (dashed).

Figure 10: The total energy as a function of time for the head-on reaction, as calculated in the *TDDM* model.

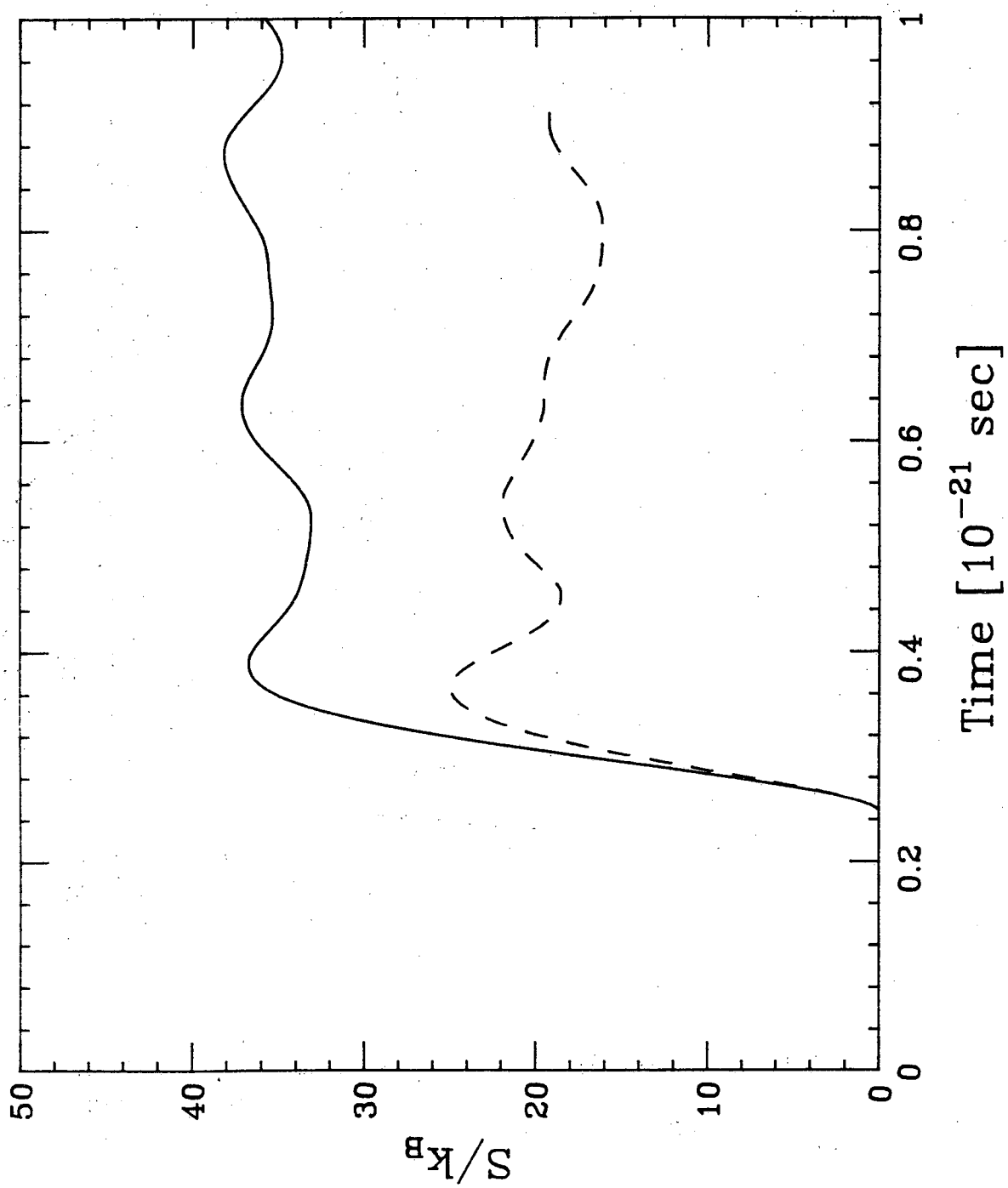

Figure 1.

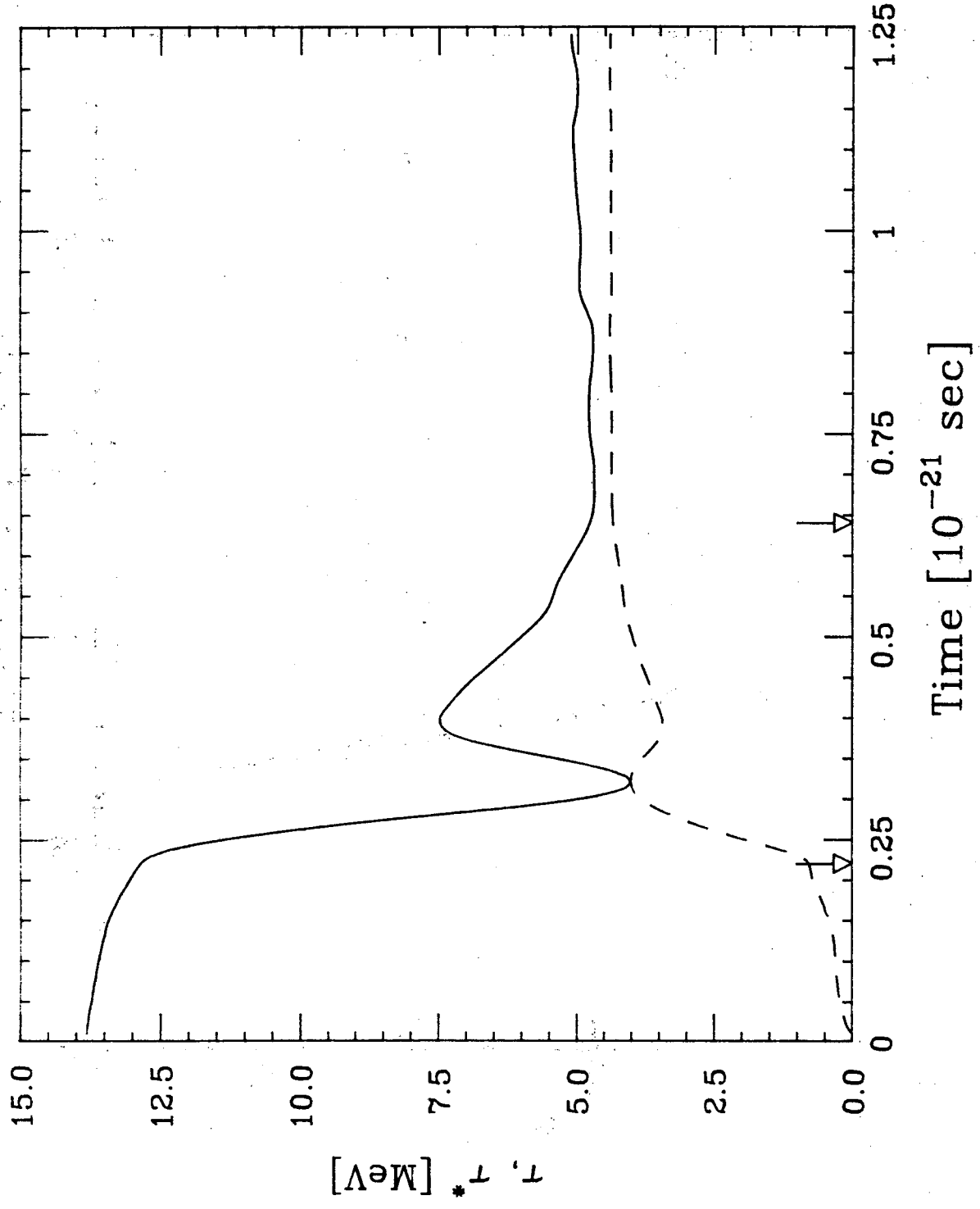

Figure 2.

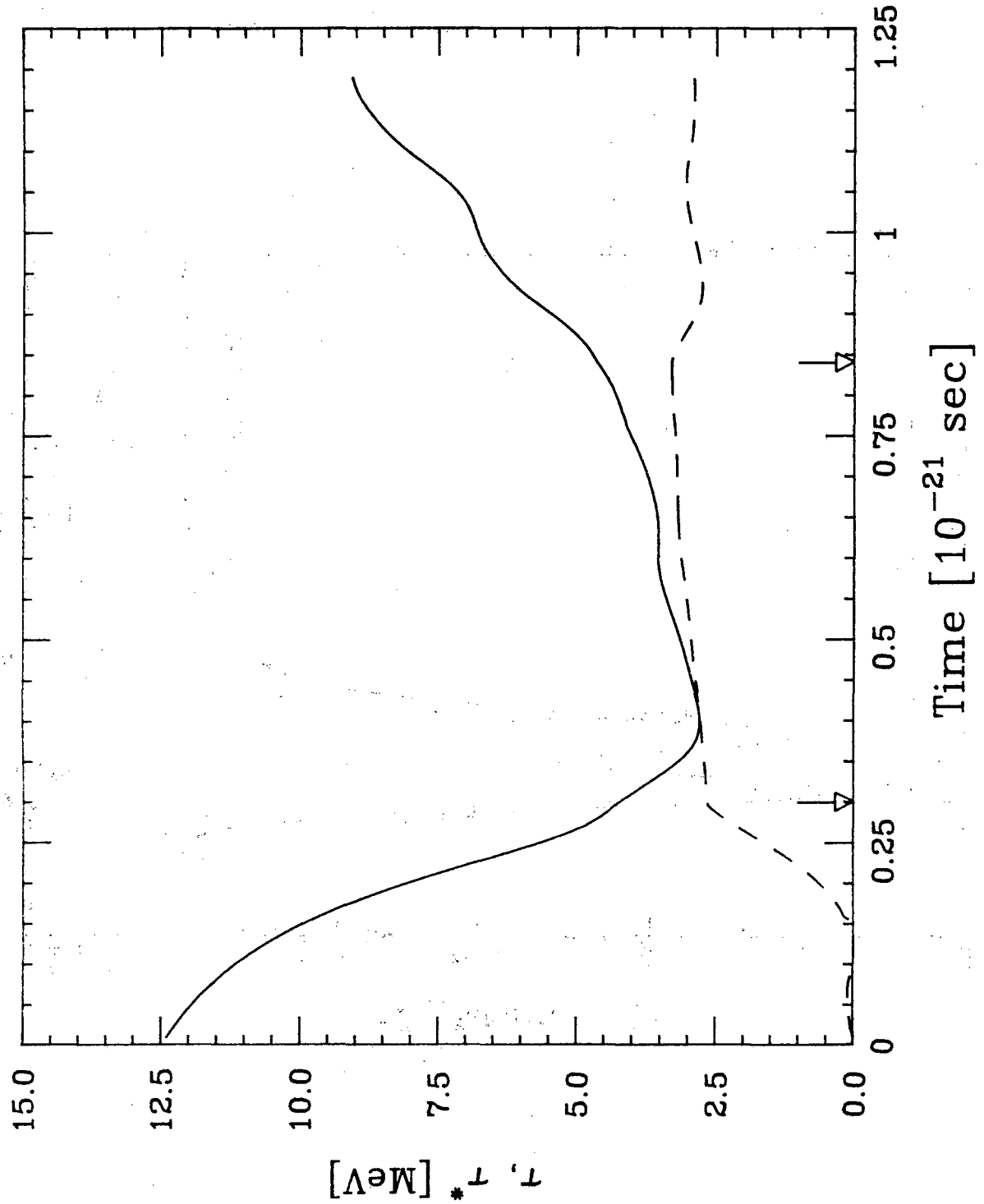

Figure 3.

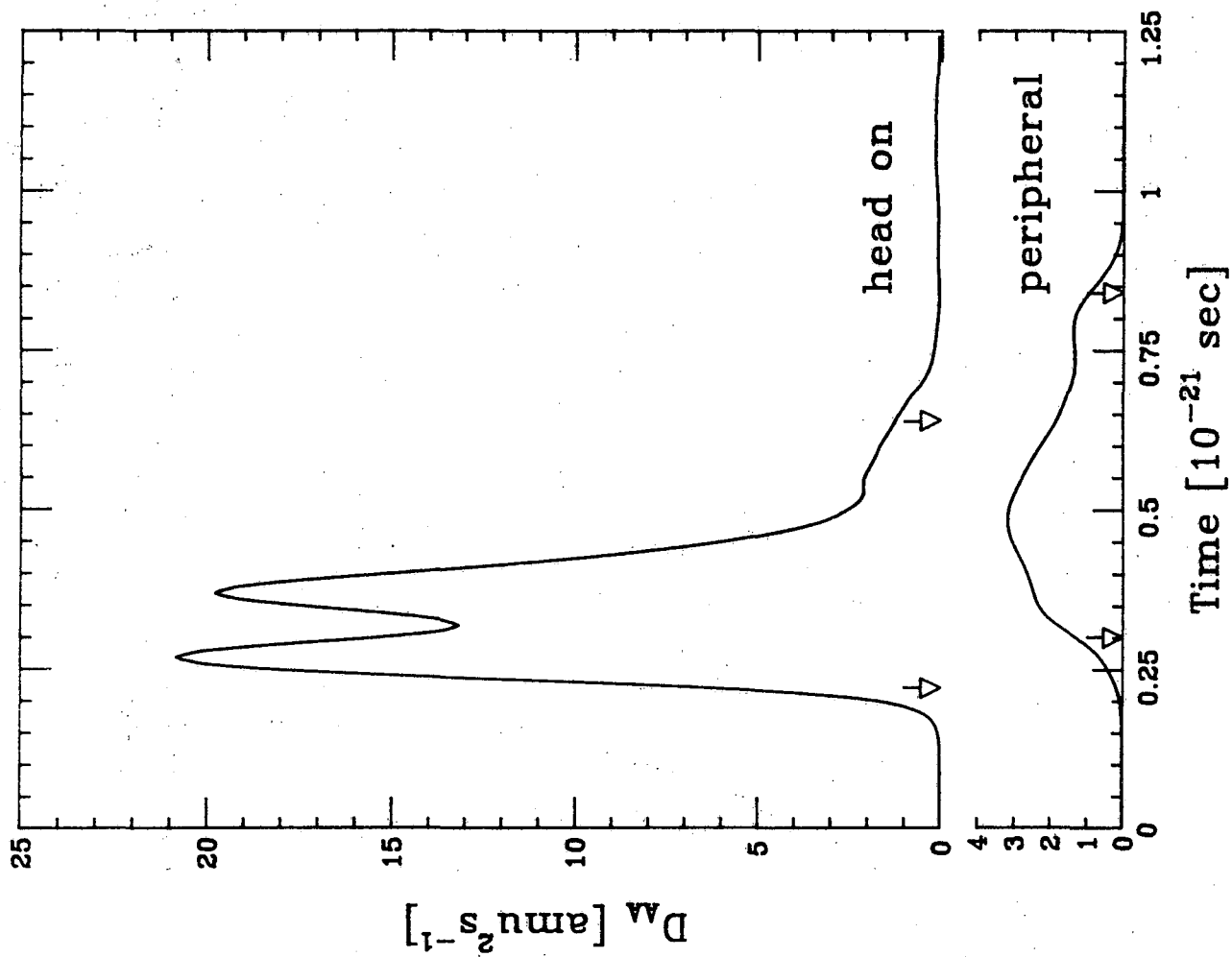
head on
peripheral
D_{AA} [amu^{2}s^{-1}]
Time [10^{-21} sec]
0
5
10
15
20
25
0
1
2
3
4
0.25
0.5
0.75
1
1.25

Figure 4.

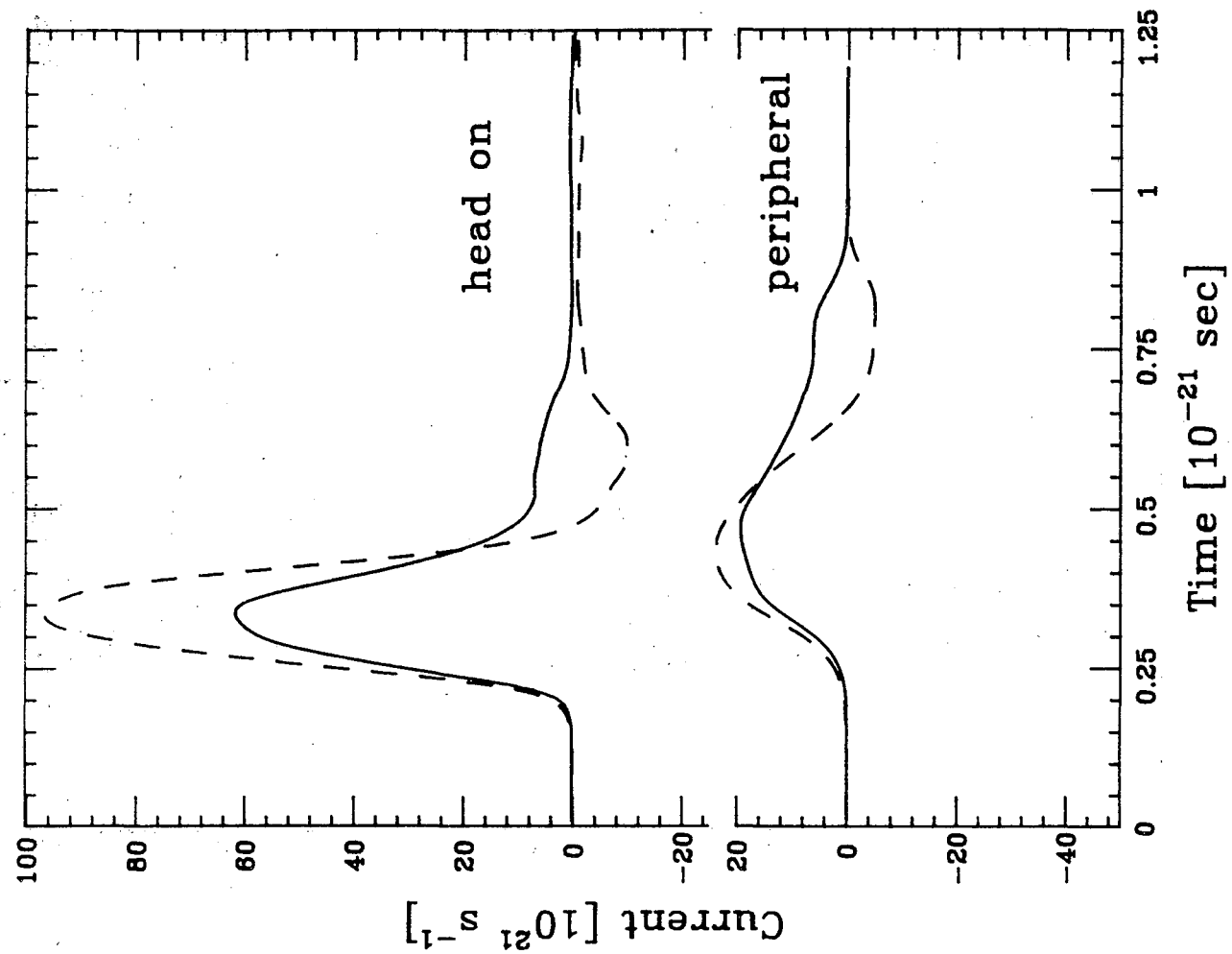
head on
peripheral
Current [10^{21} s^{-1}]
Time [10^{-21} sec]
100
80
60
40
20
0
-20
20
0
-20
-40
0
0.25
0.5
0.75
1
1.25

Figure 5.

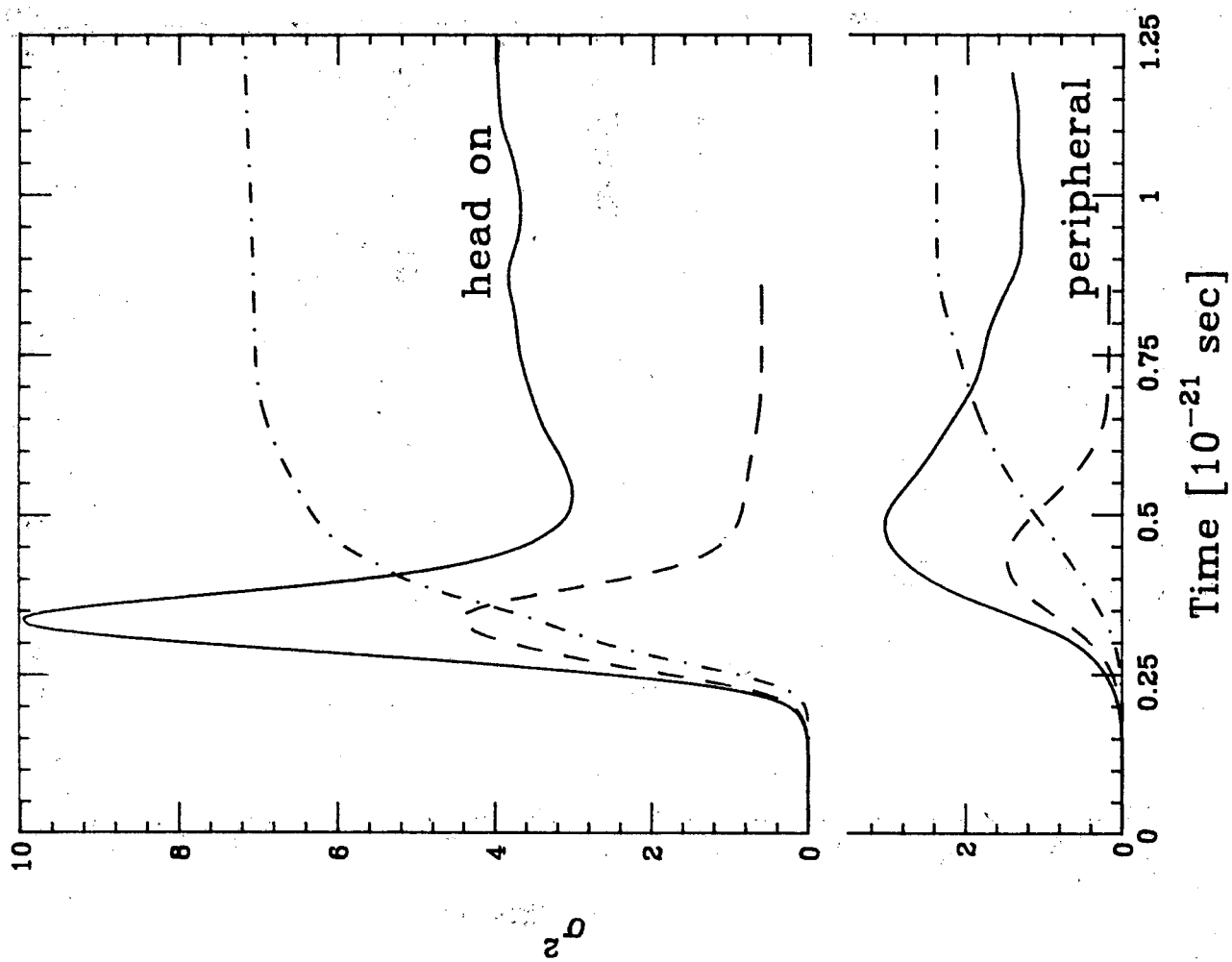
head on
peripheral
σ^2
Time [10^{-21} sec]
0
2
4
6
8
10
0.25
0.5
0.75
1
1.25

Figure 6.

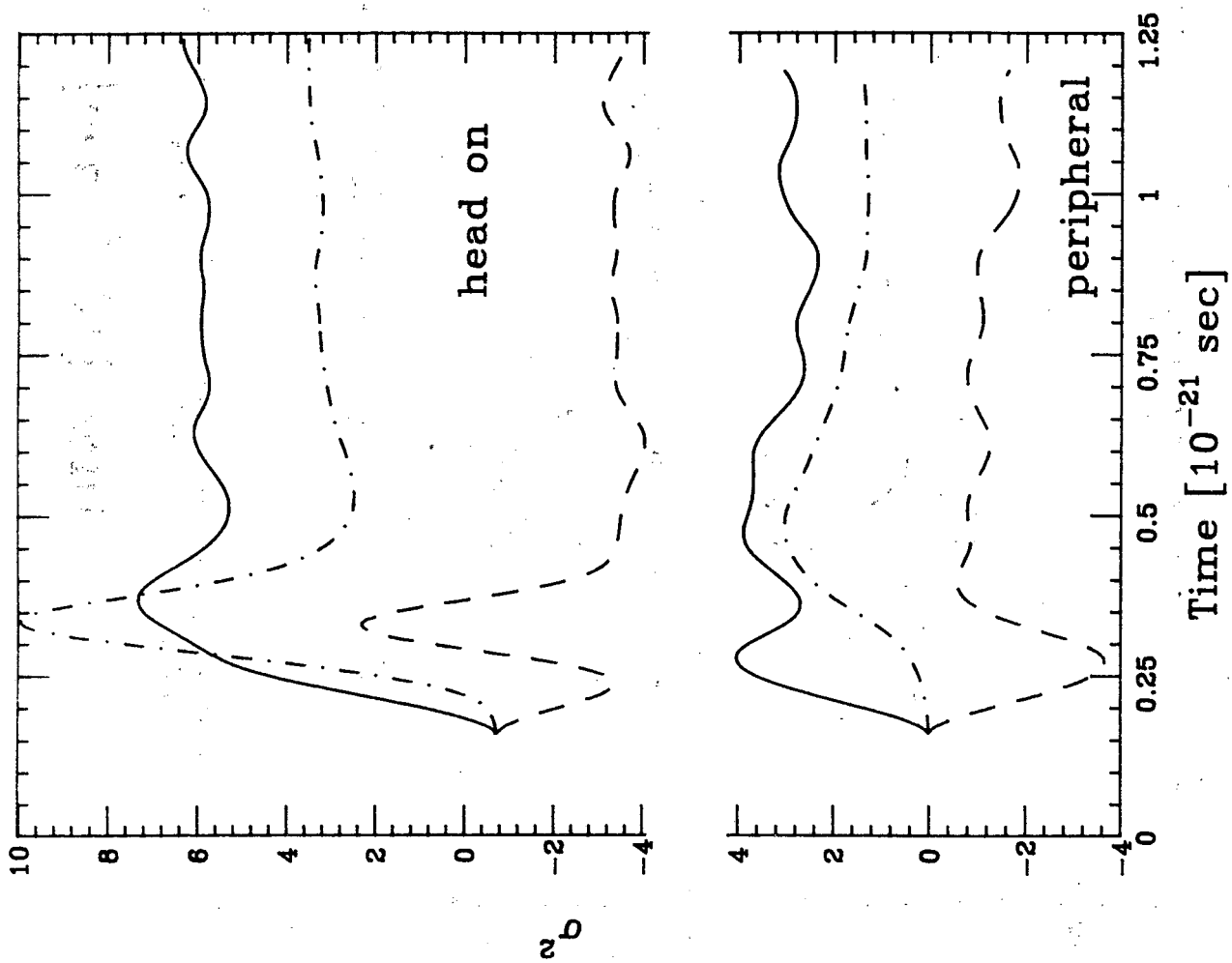
head on
peripheral
σ^2
Time [10^{-21} sec]
10
8
6
4
2
0
-2
-4
4
2
0
-2
-4
0
0.25
0.5
0.75
1
1.25

Figure 7.

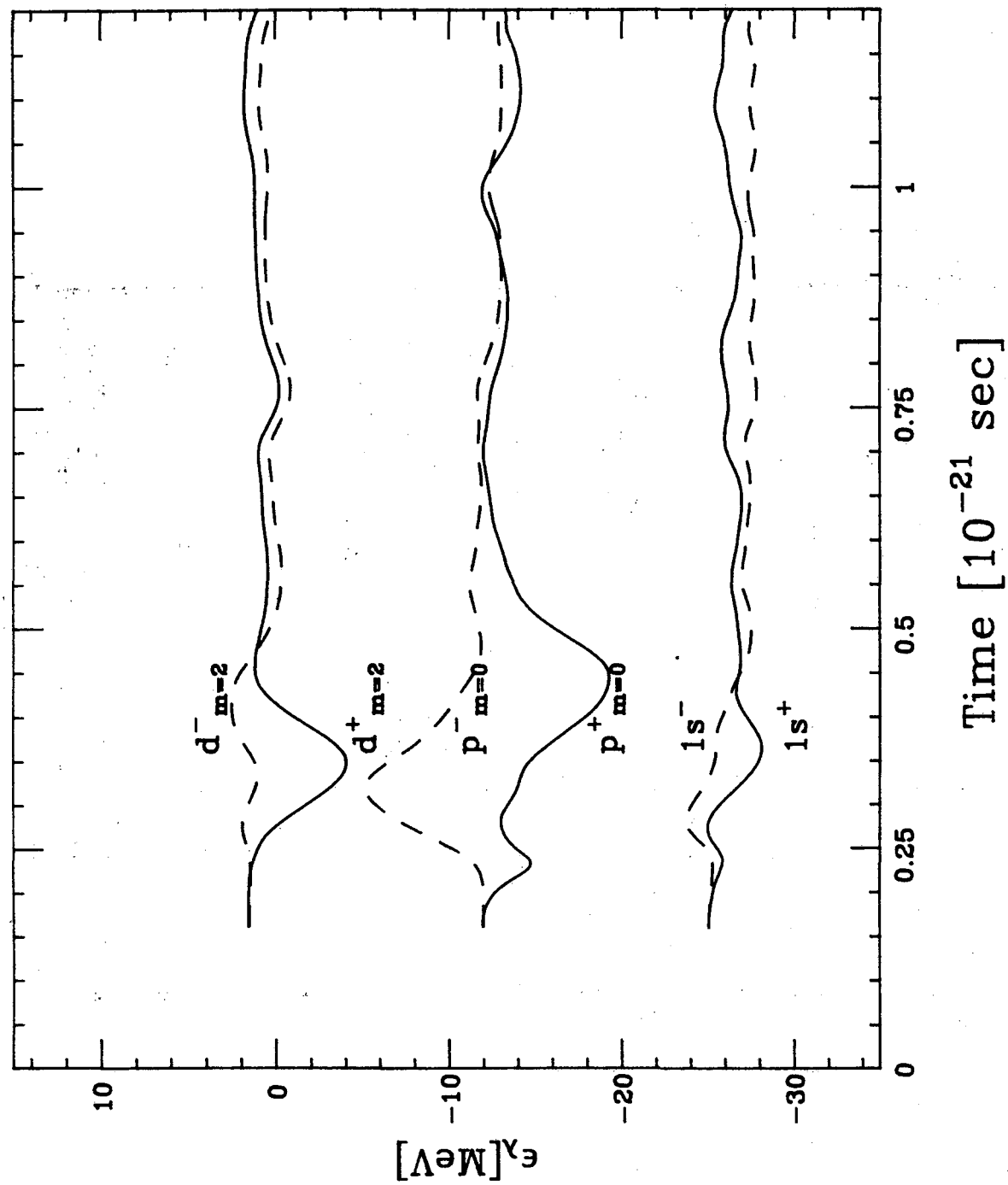
ϵ_λ[MeV]
10
0
−10
−20
−30
0
0.25
0.5
0.75
1
Time [10^{-21} sec]
$d^-_{m=2}$
$d^+_{m=2}$
$p^-_{m=0}$
$p^+_{m=0}$
$1s^-$
$1s^+$

Figure 8.

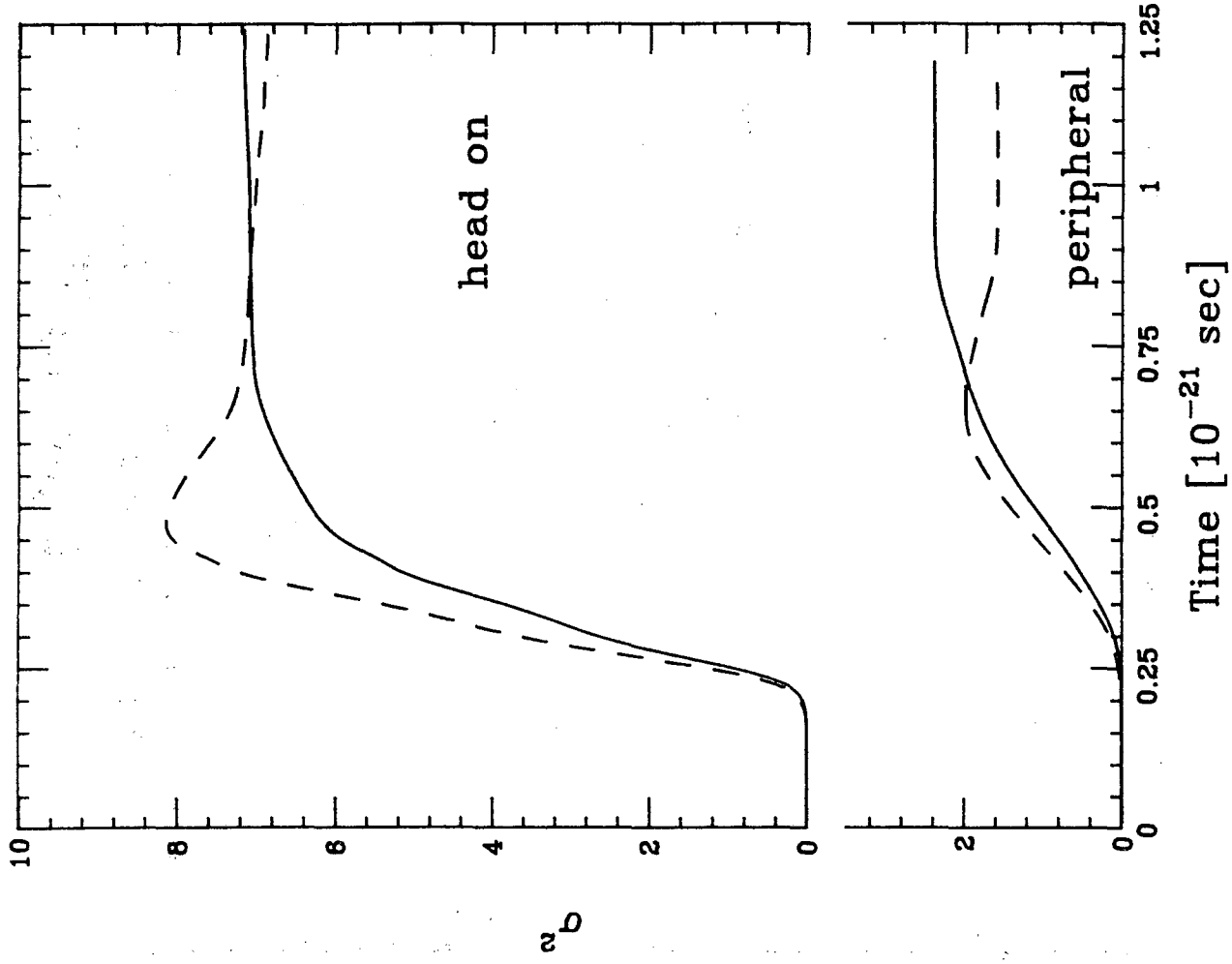
head on
peripheral
σ_2
Time [10^{-21} sec]
0
2
4
6
8
10
0.25
0.5
0.75
1
1.25

Figure 9.

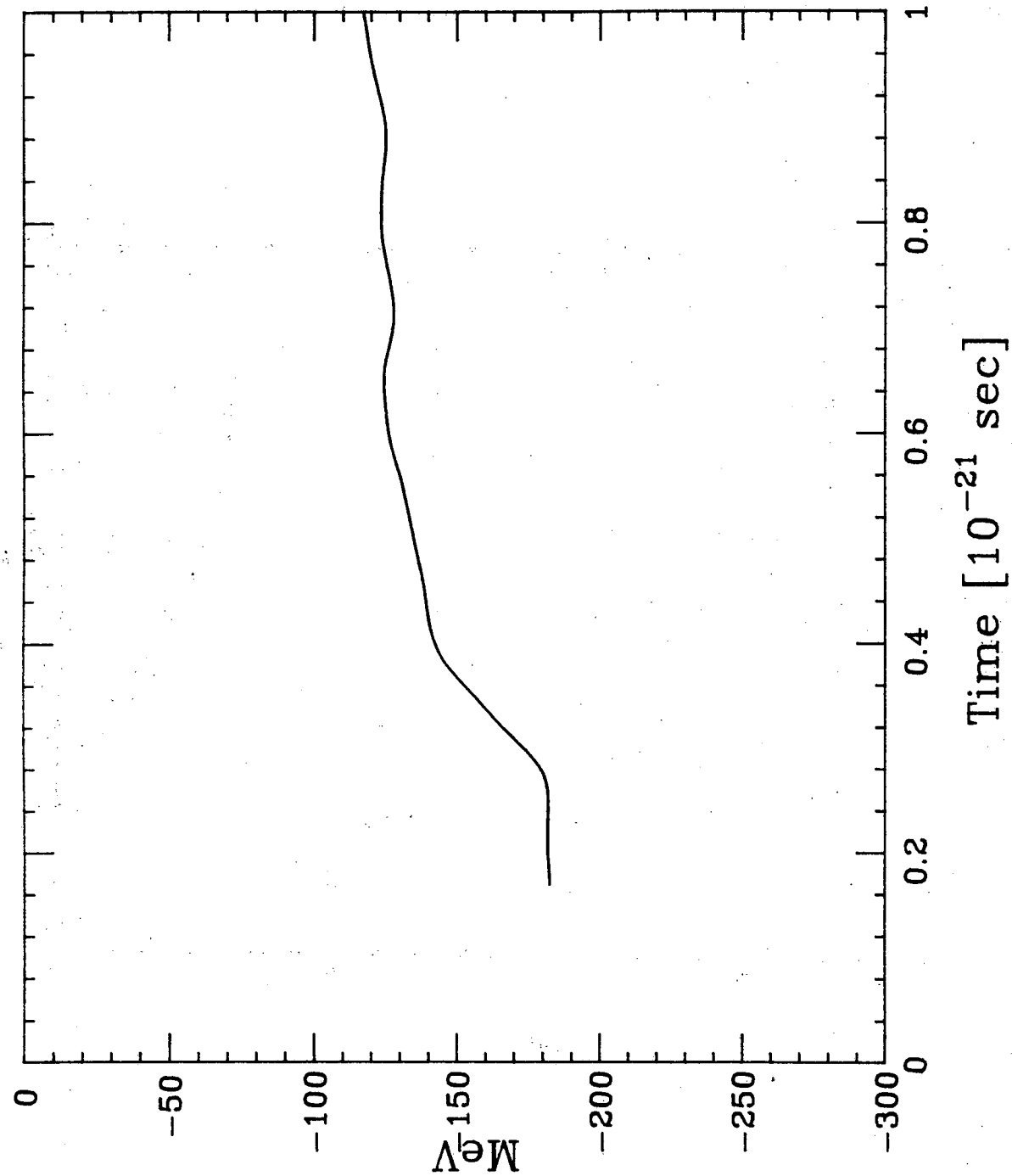

Figure 10.

LAWRENCE BERKELEY LABORATORY
TECHNICAL INFORMATION DEPARTMENT
1 CYCLOTRON ROAD
BERKELEY, CALIFORNIA 94720